Journal of ELECTRONIC MATERIALS, Vol. 47, No. 2, 2018
DOI: 10.1007/s11664-017-5919-5

Stress-Induced Resistive Switching in Pt/HfO_2/Ti Devices

GILAD ZEEVI,[1] ALEXANDER KATSMAN,[2,3] and YUVAL E. YAISH[1,4]

1.—Andrew and Erna Viterbi Faculty of Electrical Engineering, Technion, 32000 Haifa, Israel. 2.—Department of Materials Science and Engineering, Technion, 32000 Haifa, Israel. 3.—e-mail: akatsman@technion.ac.il. 4.—e-mail: yuvaly@technion.ac.il

In the present work, we study the initial SET mechanism of resistive switching (RS) in Pt/HfO_2/Ti devices under a static electrical stress and the RS mechanism under a bias sweeping mode with rates of 100 mV/s–300 mV/s. We characterize the thin HfO_2 dielectric layer by x-ray photoelectron spectroscopy and x-ray diffraction. These findings show that the layer structure is stoichiometric and nanocrystalline with a crystal diameter of $\sim$ 14 Å. We measure the temporal dependence of the conductive filament growth at different temperatures and for various biases. Furthermore, these devices present stable bipolar resistive switching with a high-to-low resistive state (HRS/LRS) ratio of more than three orders of magnitude. Activation energy $E_{RS} \approx 0.56$ eV and drift current parameter $V_0 \approx 0.07$ V were determined from the temporal dependence of the initial 'SET' process, first HRS to LRS transition [for static electrical stress of V_{DS} = (4.7–5.0 V)]. We analyze the results according to our model suggesting generation of double-charge oxygen vacancies at the anode and their diffusion across the dielectric layer. The double-charge vacancies transform to a single charge and then to neutral vacancies by capturing hot electrons, and form a conductive filament as soon as a critical neutral-vacancy cluster is formed across the dielectric layer.

Key words: Resistive switching, hafnium oxide, conductive filament, vacancies

INTRODUCTION

Resistive switching (RS) in metal–insulator-metal (MIM) devices is a phenomenon where the insulating layer resistance is tuned by applying a bias across the device. Recently, there has been new interest in this property in the field of nonvolatile resistive random access memories (RRAMs).[1] An MIM structure is one of the most attractive approaches for fabrication of high-density, high-speed and low-power RRAM. In recent years, the RS phenomenon has been observed in a wide variety of materials, such as transition metal oxides (TMOs; TiO_2,[2] Al_2O_3,[3] TaO_x[4]) and others (see review of Ref. 5). Among the TMOs, HfO_2 is a strong candidate to serve as the dielectric layer in the MIM devices due to its proven complementary metal–oxide–semiconductor (CMOS) compatibility and the encouraging results of HfO_2-based MIM devices published over the last few years.[6–8]

Several models have been proposed for the origin of RS in the distinct insulating layer materials. For the TMO group (which includes HfO_2), the physical origin of the RS phenomenon can be divided into two categories. In the first category, a Schottky barrier (SB) modulation is assumed. As a result of electrical stress, ionic charges inside the TMO dielectric layer move to form or dissolve an SB between the metallic electrode and the TMO. The second category is based on the formation/destruction of a conductive filament (CF) between two metal electrodes.[9] A widely accepted model attributes the formation of the CF in the insulating dielectric layer to vacancy aggregation. The vacancies are formed at the anode/insulating layer interface. As an oxygen is removed

(Received June 27, 2017; accepted November 4, 2017; published online November 28, 2017)

from the insulating layer into the anode, it leaves behind a doubly charged vacancy V_0^{2+}. The oxygen vacancies drift toward the cathode under electrical stress and a vacancy-containing filament grows from the cathode to the anode. Despite much theoretical work, experimental results for quantification of this initial SET process is still lacking.

In this paper, we present experimental results on the RS in Pt/HfO_2/Ti MIM devices. We believe that the origin of the RS in this case is the CF growth, as in other similar systems.[1–3,9,10] By applying distinct static electrical stress at different temperatures, we investigate the temporal dependence of a CF growth within a thin HfO_2 layer (10 nm). We use these measurements to assess the activation energy (E_{RS}) of the initial HRS/LRS transition as well as the vacancy drift current parameter, V_0. To extract these parameters, we use our suggested model, which assumes: (1) doubly charged oxygen vacancy generation; (2) their transformation to singly charged and then to neutral vacancies by capturing hot electrons; (3) diffusion of vacancies and their agglomeration to neutral vacancy clusters.

EXPERIMENT

MIM Device Fabrication

The structure of our Pt/HfO_2/Ti MIM device is depicted in Fig. 1. We use a standard photolithography process and an electron beam evaporator to form Cr/Pt bottom electrodes on top of a P^{++} silicon wafer capped with 285 nm of SiO_2. A thin HfO_2 dielectric layer (thickness $\sim$ 10 nm) was deposited by atomic layer deposition (ALD) at 270°C and a pressure of 0.046 kPa, with a hafnium precursor, tetrakis(dimethylamino)hafnium (TDMAH) from Strem Chemicals, Inc. Additional deposition parameters were the following: bubbler temperature = 75°C, pulse = 0.5 s, wait = 7 s, H_2O at room temperature, pulse = 1 s, wait = 12 s. The deposition rate was 0.076 nm/cycle. Top electrodes of Ti/Au were deposited on the hafnia layer in similar procedure as the bottom electrodes. Our MIM capacitors were fabricated in three sizes (surface area), 784 μm^2, 4900 μm^2, and 14,400 μm^2. For the characterization of the HfO_2 layer, we used x-ray photoelectron spectroscopy (XPS) and grazing incidence x-ray diffraction (GIXRD). The XPS was acquired by a Thermofischer sigma probe. The survey collection angle was 54° ± 30° with a pass energy of 200 eV, while the high-resolution scans were taken at the same angle and pass energy of 50 eV. For the XPS analysis, we used XPSPEAK 4.1. The x-ray diffraction (XRD) 2θ measurement were taken by a Rigaku Smartlab, with a target of: Cu K-alpha 9Kw rotating anode. For the GIXRD, we used a Rikagu SmartLab high-resolution diffraction system. The 2θ scan was performed at a 0.9° grazing angle (extracted from diffraction measurement), with Ka x-ray (wave length = 1.54 Å).

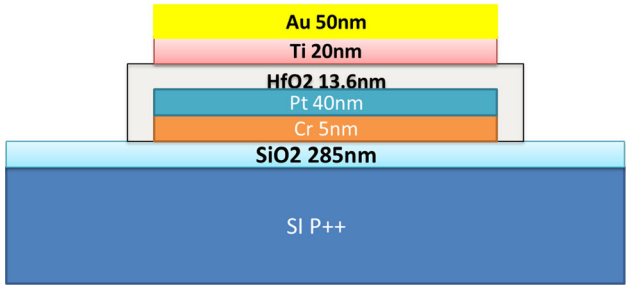

Fig. 1. MIM capacitor schematic: the devices were fabricated on top of a Si/SiO_2 (285 nm) wafer with Cr/Pt bottom electrodes, HfO_2 dielectric layer and Ti/Au top electrodes; the capacitors were fabricated with various sizes of $282^2 \mu m^2$, 70^2 μm^2, and 120^2 μm^2.

Electrical Measurements

We performed temporal dependence measurements of stress-induced breakdown in the MIM capacitors. The device top electrode was connected to a programmable power source (Yokogawa 7651), while the bottom electrode was connected to data acquisition (DAQ) through a Stanford Research Systems RS570 LNA. We placed the devices on a hot plate, and for each SET of electrical measurements with a constant temperature (temperature ranges between 293 K and 373 K) we varied the bias voltage and recorded the current flowing through the capacitor dielectric layer. When a CF was created, the current showed a sharp rise; at this moment, the electrical stress was quickly relieved. The time (t_{RS}) between the initial bias stress and the moment of sudden current rise was registered. This time interval, named delay time, represents the duration needed for complete CF growth across the capacitor's dielectric layer. We also checked the RS characteristics on similar MIM devices. In these measurements, the bottom electrode was always connected to the ground and the voltage on the top electrode was swept at rates between 100 mV/s and 300 mV/s. The bias was first swept to a positive value. After the initial SET stage at bias $\sim$ 4.5 V, our device switched its resistive state at a bias of 1 V for SET (to low resistive state, LRS) and at − 1.5 V for RESET (back to high resistive state, HRS).

RESULTS

ALD HfO_2 Layer Characterization

The XRD results of the deposited HfO_2 layer show two broad diffraction peaks at 31.73° and 52.37° (Fig. 2a), which are typical of an amorphous hafnia layer.[12,13] Nevertheless, by zooming in on the predominant peak at 2θ = 31.73°, we extract data on the nano-crystallinity of the HfO_2 layer. Using XPSPEAK 4.1 software, we fit Gaussian/Lorentzian curves (Fig. 2b) to the XRD data between 2θ = 23° to 38°. The best fit includes two peaks, which belong to the hafnia monoclinic phase (111) and (− 111); PDF 00-034-0104. The nano-crystallite size is

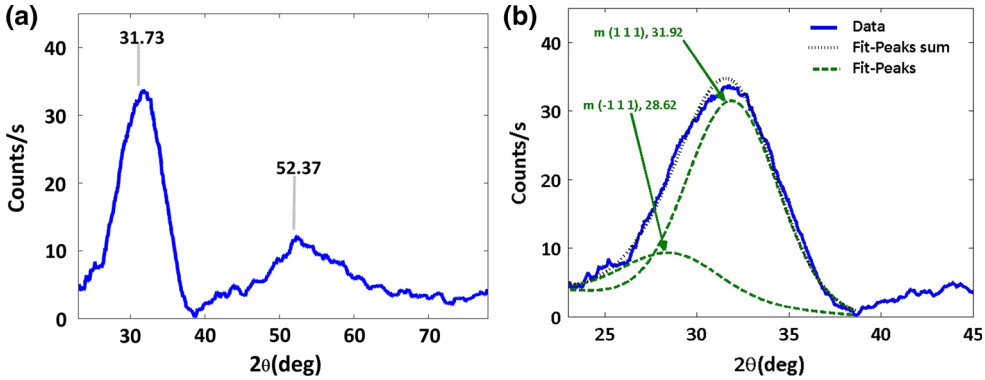

Fig. 2. XRD measurements of the 13-nm-thick HfO_2 layer: (a) the wide spectra scan of the thin HfO_2 layer shows two broad diffraction peaks centered at 2θ = 31.73° and 2θ = 52.37°; we associated the peak at 2θ = 52.37° with a mix of orthorhombic and monoclinic hafnia nano-crystals (see text), while the peak at 2θ = 31.73° is with (1 1 1) and (− 1 1 1) peaks of the monoclinic phase; (b) fitting to the peak at 2θ = 31.73°; zooming in on the scan area between (23÷45)° shows the fit of two Lorentzian/Gaussian peaks centered at 28.62° [m(− 1 1)] and 31.92° [m(1 1 1)]; we use the dominant peak (31.92°) to extract the HfO_2 nano-crystalline size.

estimated from the line broadening of the (111) peak using the Scherrer equation[11]:

$$D(2\theta) = \frac{K\lambda}{\beta \times \cos(\theta)} \quad (1)$$

where D is the crystallite diameter, K is a dimensionless shape factor, λ is the x-ray wavelength, β is the peak full width at half maximum (FWHM, in radian) and θ is the diffraction angle. In our measurements, λ = 0.154 nm and β = 0.1 rad. With $2\theta = 31.92°$, and taking K = 0.9, the result is a crystallite diameter of $D \approx 1.43$ nm. As for the peak centered at 2θ = 52.37°, we attribute it to an even smaller nano-crystal mix of orthorhombic phase peaks (4 0 2) and (4 2 1)—PDF 01-083-0808—and monoclinic-phase peak (0 2 2); PDF 00-034-0104.

The XPS survey scan depicted in Fig. 3a shows an HfO_2 layer stoichiometry with an O-to-Hf ratio of 2.04:1. For measurement calibration, we calculated a shift in the energy scale of 6.09 eV from the C1s peak (Fig. 3b) by setting the contaminating carbon peak at 284.5 eV. The high-resolution XPS scan revealed Hf4f peaks (Fig. 3c) positioned at 16.641 eV and 18.314 eV with a FWHM of 1.51 eV and 1.376 eV, respectively, that corresponds to ~ 1.66-eV spin–orbit doublet separation.[15] The curve fitted by XPSPEAK 4.1 is a Lorentzian/Gaussian mix, with a peak area ratio (after background removal) of ~ 0.73. These results show a stoichiometric HfO_2 thin layer clear of sub-oxides[14,15]. Peaks associated with the oxygen 1S orbital are presented in Fig. 3d. The major peak at 530 eV corresponds to an Hf–O bond in the HfO_2, while the small secondary peak at 532.3 eV lies between the Hf–O bond of the HfO_2 and the Si–O bond of the SiO_2 (532.9 eV).

RS Under Static Electrical Stress

We examined the initial CF formation by applying a constant electrical stress at a constant temperature on our MIM devices, and by recording the temporal electrical current variation. Each measurement was performed on different (pristine) MIM device. All devices were similar to each other. Figure 4a depicts I_{ds} measurements for various biases (V_{ds}) at constant temperature of 313 K. The time elapsed between the moment of turning on the electrical stress V_{ds} until a sharp current surge is observed (delay time t_{RS}), decreasing as the bias grows. For V_{ds} = 4.5 V, no significant change in I_{ds} was observed for over 25 min after the bias was turned on. Another view of our results is presented in Fig. 4b, where I_{ds} is measured for various temperatures at a constant bias (4.7 V). We detected no significant change in the current at 293 K (even after more than 25 min), while from 313 K and above, the HRS/LRS transition was observed, and as the temperature increased, t_{RS} becomes shorter.

The temporal dependencies of the CF formation on temperature and static electrical stresses are summarized in Fig. 5. The period t_{RS} is depicted in natural logarithm scale, and the linear fit of the data allows us to extract the relevant parameters of the model: the activation energy (E_{RS}) and the drift current parameter, V_0. The measured values of t_{RS} are analyzed based on the expression:

$$t_{RS} \sim \exp\left(\frac{E_{RS}}{k_B T}\right) = \exp\left[\frac{E_a^*}{k_B T} - \frac{V}{V_0}\right], \quad (2)$$

The extracted values $E_{RS} \approx 0.56$ eV, $V_0 \approx 0.07$ V and $E_a^* = 2.5 \pm 0.2$ eV are further reviewed in the discussion section below.

Resistive Switching at Sweeping Mode

RS in our Pt/HfO_2/Ti devices was SET by sweeping V_{ds} from zero up to + 5.2 V, then down to − 5.8 V and back to 0 V, at a rate of 300 mV/s. Following the initial SET, 'Inset' step, a stable RS

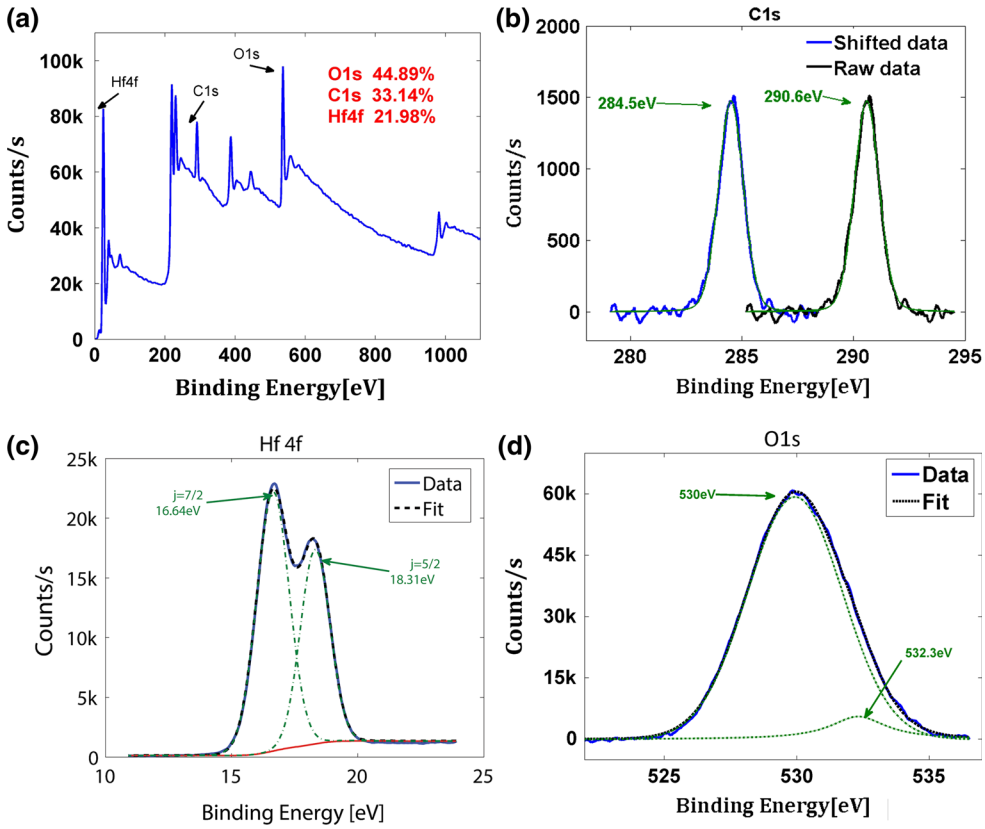

Fig. 3. XPS measurements on 13-nm ALD-grown HfO_2 on top of a SiO_2 surface: (a) survey scan; the hafnium/oxygen percentage ratio shows a stoichiometric HfO_2 layer; (b) the C1 s peak is used to calibrate the measurements; the known peak location is at 284.5 eV; (c) the peaks associated to the Hf4f orbitals: peak positions at 16.641 eV and 18.314 eV correspond to $\sim$ 1.66-eV spin–orbit doublet separation; (d) oxygen-associated peaks: the major peak at 530 eV corresponds to an Hf–O bond in the HfO_2, while the small secondary peak at 532.3 eV lies between the Hf–O bond of the HfO_2 and the Si–O bond of the SiO_2 (532.9 eV).

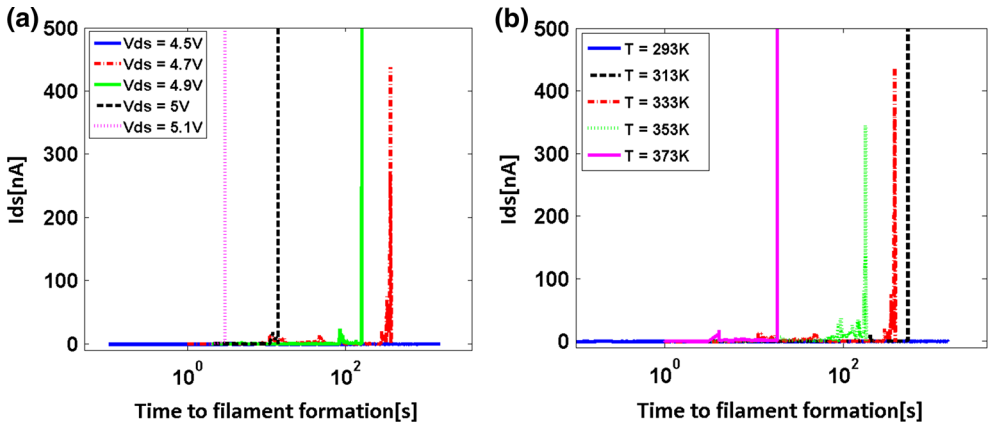

Fig. 4. Temporal dependence of CF formation: (a) variation of I_{ds} under different static electrical stresses and constant temperature of 313 K; (b) I_{ds} measurements at different temperatures under a constant bias of 4.7 V.

behavior was obtained with reversible transition from a HRS to a LRS by sweeping V_{ds} between 1.2 V to − 1.5 V (Fig. 6). Our SET and RESET voltages (1 V and − 1.2 V, respectively) are well correlated with those voltages of similar devices (10-nm HfO_2 and Ti top electrode).[10] Additionally, our devices demonstrate stable RS behavior with an HRS-to-LRS ratio of over three orders of magnitude, and the RS behavior showed no dependence on device area (this behavior corresponds to the formation of a CF path). Furthermore, our devices are comprised of a quasi-amorphous HfO_2 dielectric layer, and their good performance is contrary to the results of Lanza et al.[16] where a good bipolar RS was achieved only

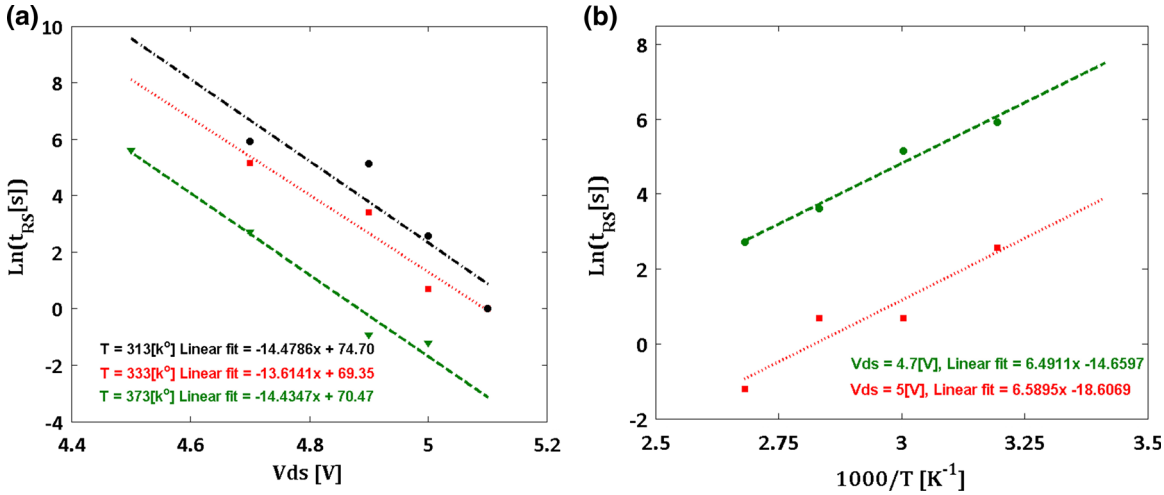

Fig. 5. Temporal dependence of CF growth during stress-induced RS: (a) the delay time, t_{RS}, as a function of electrical stress, V_{ds}, at a constant temperature; the linear fits for different temperatures (circles for 313 K, squares for 333 K and triangles for 373 K) can be distinguished by their color; (b) the delay time, t_{RS}, as a function of temperature at a constant V_{ds}. Linear fits along with their equations, green circles for V_{ds} = 4.7 V, and red squares for V_{ds} = 5.1 V (Color figure online).

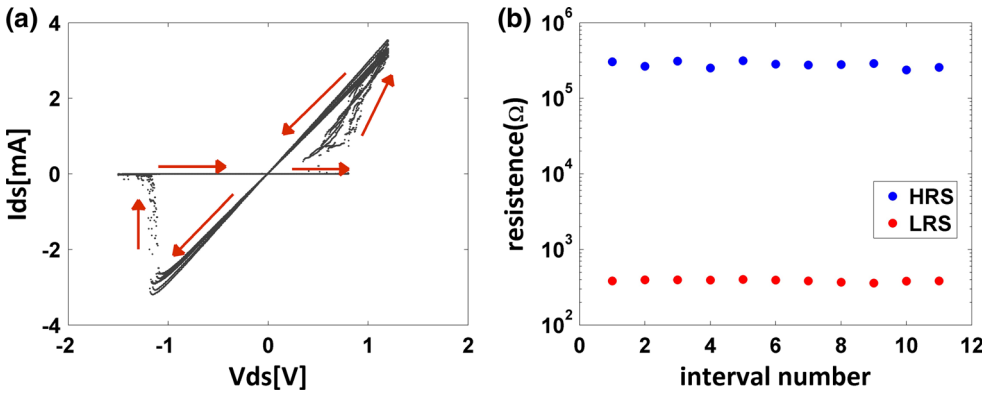

Fig. 6. Stable RS behavior of the fabricated Pt/HfO_2/Ti devices: (a) RS after initial SET, 'Inset', the device switches from HRS to LRS at V_{ds} = 1.2 V (SET), and back from LRS to HRS at V_{ds} = − 0.5 V; (b) stable HRS and LRS values were achieved, with the HRS-to-LRS ratio close to three orders of magnitude. The resistance is calculated at Vsd = − 0.2 V.

after crystallization of the HfO_2 film by mild annealing at ∼ 400°C.

DISCUSSION

Temperature and bias dependencies of the HRS/LRS delay time, t_{RS}, were analyzed by Gonon et al. [1] in their study of RS in Au/HfO_2/(Pt, TiN) devices, with the HfO_2 layer deposited by ALD. At the constant voltage stress (CVS) mode with V_{ds} = 3 V, they found that the delay time is thermally activated with an activation energy of 1.05 eV, which is exponentially varied with the applied stress voltage V: $t_d \sim \exp(-V/V_0)$, where the drift current parameter V_0 = 0.21 V (at T = 358 K). Assuming the delay time is inversely proportional to the vacancy diffusion coefficient, $t_{RS} \sim D_V^{-1} = D_0^{-1}\exp(E_a/kT)$ with $E_a = E_{a0} - qF\boldsymbol{s}$, $\boldsymbol{s}$ is the vacancy hopping distance, and F is the applied electric field, they found $E_{a0} \approx$ 1.5 eV (E_{a0} is the intrinsic energy barrier for vacancy hopping in the absence of an electric field). This activation energy corresponds to diffusion of V_O^+ in HfO_2. However, the delay time t_{RS} originates from at least three possible factors: doubly charged vacancy generation rate (G), the vacancy drift velocity ($\bar{V}$) and the density of free electrons injected at the cathode,[17] which controls the transformation rate of charged vacancies to neutral ones forming vacancy clusters. Following the model developed in our previous work,[17] we assume that transition from the HRS to a LRS corresponds to appearance of a vacancy cluster of a critical size N. The percolation conductive pass for electrons can be formed by an N-vacancy cluster with $N \sim d/a$, where a is the interatomic O–O distance in hafnia, and d is the insulating layer thickness. The concentration of N–V clusters should reach a certain value, when at least one such cluster appears in the system:

$$n_{NV}^{0\ldots0}\Delta V = 1 \qquad (3)$$

where ΔV is the volume of hafnia where generation of vacancies occurs. The time needed to reach this concentration, t_{RS}, can be found from the following expression[17]:

$$t_{RS} = \left(\frac{N!}{\Delta V n_V^0}\right)^{1/N} \left(\frac{1}{\beta' n_f}\right)^{\frac{N-2}{N}} \left(\frac{1}{n_V^0}\right)^{1/N} \left(\frac{1}{\theta n_V^+}\right)^{\frac{N-2}{N}} \quad (4)$$

where n_V^0 and n_V^+ are the quasi-stationary concentrations of neutral and singly charged vacancies, n_f is the density of free electrons injected by cathode, β' is the capture rate of free electrons by vacancy traps V_O^+; according to Mannequin et al.,[18] $n_f = n_f^0 \exp(A \times V)$, where V is the electrical stress, A is the interface-dependent constant; θ is the rate of bi-vacancies formation, $\theta = D_{V^+}/\lambda^2$, D_{V^+} is the diffusion coefficient of V_O^+ and λ is the jump length of the vacancies. Using expressions for quasi-stationary concentrations of vacancies found in,[17] one can write:

$$t_{RS} = \left(\frac{N!}{\Delta V}\right)^{1/N} \left(\frac{\theta\beta'}{\beta\tau_0}\right)^{2/N} \left(\frac{\beta K}{\alpha}\right)^{1/2} \left(\frac{1}{\beta' n_f}\right) \left(\frac{\tau_0}{\theta n_V^{2+}}\right)^{1/2} \quad (5)$$

where β is the capture rate of free electrons by vacancy traps V_O^{2+}, n_V^{2+} is the quasi-stationary concentration of doubly charged vacancies, which are generated at the cathode and then diffuse and transform to singly charged vacancies, and $\tau_0 = \tau_{00} \exp(\Delta E/k_B T)$ is the lifetime of an electron in a neutral vacancy. As can be seen, for $N \gg 1$, the temperature dependence of t_{RS} is determined mainly by the last factor. According to our previous results [17]:

$$\begin{aligned} n_V^{2+} &= \frac{G}{\bar{V}}\left[1 - \exp\left(-\frac{\bar{V}(d-x)}{D_{V^{2+}}}\right)\right] \\ &\approx \bar{n}_{V0}^{2+} \exp\left(-\frac{E_a - bF - E_{V^{2+}}}{kT}\right) \end{aligned} \quad (6)$$

where $G = G_0 \exp[-(E_a - bF)/k_B T]$, $\bar{V} = (2qFD_{V^{2+}}/k_B T)$ and $D_{V^{2+}}$ are the generation rate, the drift velocity under electric field F, and the diffusion coefficient of doubly charged vacancies, respectively, b is the bond polarization parameter, q is the electron charge, and $\bar{n}_{V0}^{2+} = (k_B T G_0/2qFD_{V0}^{2+})$. Substituting $\bar{V}$, θ and τ_0, one can write:

$$\begin{aligned} t_{RS} &= t_{RS}^0 \exp\left[\frac{E_{RS}}{k_B T}\right] \\ &= t_{RS}^0 \exp\left[\frac{E_a - bF - AV - E_{V^{2+}} + (E_{V^+} + \Delta E)(1 - 4/N)}{2k_B T}\right] \end{aligned} \quad (7)$$

where $t_{RS}^0 \approx \left(\frac{\lambda}{n_f^0}\right)\left(\frac{N!}{\Delta V}\right)^{1/N}\left(\frac{2qFK\tau_{00}}{k_B T \alpha \beta G_0}\right)^{1/2}$. This expression can be represented as Eq. 2, where $E_{RS} = E_a^* - k_B T \times V/V_0$ with the following parameters:

$$E_a^* = \frac{E_a - E_{V^{2+}} + (E_{V^+} + \Delta E)(1 - 4/N)}{2}, \quad (8a)$$

$$V_0 = 2k_B T d/(b + 2Ak_B T d) \quad (8b)$$

Let us compare these theoretical values with the ones extracted from our experiments (Fig. 5).

The migration activation energies of oxygen vacancies were extracted from the measurement data[19] and obtained from ab initio calculations,[20] E_{V^+} = 1.5 eV, $E_{V^{2+}}$ = 0.7 eV; the value of bond energy E_a = 4.4 eV was found from the breakdown voltages[19]; the binding energy of an electron in a neutral vacancy can be evaluated as $\Delta E = (0.1 - 0.2)$ eV. For $N = 30 - 50$, one can obtain from Eq. 8a $E_a^* = (2.49 - 2.63)$ eV, which is in excellent agreement with the value obtained from the experimental data (E_a^* = 2.5 ± 0.2 eV) depicted in Fig. 5.

In order to find parameter V_0, we should first evaluate the bond polarization parameter, b. This parameter was calculated based on the thermochemical description of dielectric breakdown in high-dielectric constant materials using the expression $b = p_0 q(2 + \kappa)/3$.[21] For HfO_2, $\kappa \sim 25$ and p_0 = 1.02 for cubic hafnia and p_0 = 0.44 for tetragonal hafnia[21]. The first value results in $b = 9q$ nm, and the second in $b = 4q$ nm. The value of the parameter A for a TiN/HfO_2 interface has been measured using a stress-induced leakage current (SILC).[18] According to Ref. 18, SILC follows a law $I_{SILC} \sim Kt^n$, where the exponent n is around 1.15 and $K \sim \exp(A \times V)$ with A = 3.86 V^{-1}. Using the experimental value $V_0 \approx 0.07$ V and the hafnia layer thickness d = 10 nm, for temperatures 313–373 K, one can obtain: $b = 2k_B T d(V_0^{-1} - A) \approx (5.6 - 6.7)q$ nm. This result seems to be very reasonable for the bond polarization parameter in nano-crystalline hafnia film.

Therefore, RS in the fabricated Pt/HfO_2/Ti devices is well described as thermally activated, and the stress influenced growth of a CF across the dielectric layer. The activation energy of the process is a combination of several activation energies responsible for different processes involved in the filament formation: generation of new oxygen vacancies, diffusion of doubly charged and singly charged vacancies, and binding energy of electrons in neutral vacancies. Polarization of atomic bonds under electrical stress facilitates the vacancy generation and is responsible for the bias dependence of the activation energies. Transformation of doubly charged and singly charged vacancies into the neutral ones is a necessary condition for agglomeration of vacancies. This transformation is controlled by capture of hot

electrons injected from the cathode; the latter is also bias-dependent.

CONCLUSION

RS in Pt/HfO_2/Ti devices, where the hafnia layer was deposited using an ALD apparatus, was studied under static electrical stresses and bias sweeping mode with different rates between 100 mV/s and 300 mV/s. The devices show a stable bipolar RS with a high-to-low resistive state (HRS/LRS) ratio of more than three orders of magnitude. RS under static electrical stress was examined for temperature and bias dependencies. The activation energy of the process decreases with the applied bias according to $E_{\mathrm{RS}} \approx E_a^* - k_B T \times V/V_0$ with $E_a^* = 2.5 \pm 0.2$ eV and $V_0 \approx 0.07\,V$. The results were analyzed in the framework of the model, suggesting CF growth across the dielectric hafnia layer. The CF is built from the vacancies generated at the anode. The doubly charged vacancies diffuse across the dielectric layer, transform to singly charged and neutral vacancies by capturing hot electrons and form a CF as a critical neutral vacancy cluster across the dielectric layer. The measured effective activation energy is a combination of different activation energies responsible for separate stages of the total process [Eq. 8a]. Since the individual activation energies for different vacancies in hafnia are well established, the effective activation energy for RS was calculated and found to be in a good agreement with the measured value. The bias dependence of the activation energy is explained mainly by polarization of atomic bonds under electrical stress, which facilitates the vacancy generation. At the same time, the electrical stress influences diffusion of charged vacancies and injection of electrons from the cathode, both factors reinforcing bias dependence of the RS.

REFERENCES

1. P. Gonon, M. Mougenot, C. Vallée, C. Jorel, V. Jousseaume, H. Grampeix, and F. El Kamel, *JAP* 107, 074507 (2010).
2. H. Mähne, S. Slesazeck, S. Jakschik, I. Dirnstorfer, and T. Mikolajick, *Microelectron. Eng.* 88, 1148 (2011).
3. Y. Wu, S. Yu, B. Lee, and P. Wong, *JAP* 110, 094104 (2011).
4. M.J. Lee, C.B. Lee, D. Lee, S.R. Lee, M. Chang, J.H. Hur, Y.B. Kim, C.J. Kim, D.H. Seo, S. Seo, U.I. Chung, I.K. Yoo, and K. Kim, *Nature Mater.* 10, 625 (2011).
5. K.M. Kim, D.S. Jeong, and C.S. Hwang, *Nanotechnology* 22, 254002 (2011).
6. J.W. Yoon, J.H. Yoon, J.H. Lee, and C.S. Hwang, *Nanoscale* 6, 6668 (2014).
7. R. Zazpe, M. Ungureanu, F. Golmar, P. Stoliar, R. Llopis, F. Casanova, D.F. Pickup, C. Rogerofh, and L.E. Hueso, *J. Mater. Chem. C* 2, 3204 (2014).
8. K.L. Lin, T.H. Hou, J. Shieh, J.H. Lin, C.T. Chou, and Y.J. Lee, *JAP* 109, 084104 (2011).
9. M. Lanza, *Materials* 7, 2155 (2014).
10. T. Bertaud, D. Walczyk, Ch Walczyk, S. Kubotsch, M. Sowinska, T. Schroeder, Ch Wenger, C. Vallée, P. Gonon, C. Mannequin, V. Jousseaume, and H. Grampeix, *Thin Solid Films* 520, 4551 (2012).
11. J.I. Langford and A.C. Wilson, *J. Appl. Cryst.* 11, 102 (1978).
12. M.-Y. Ho, H. Gong, G.D. Wilk, B.W. Busch, M.L. Green, P.M. Voyles, D.A. Muller, M. Bude, W.H. Lin, A. See, M.E. Loomans, S.K. Lahiri, and I. Petri, Räisänen. *JAP* 93, 1477 (2003).
13. Y.-Q. Chang and W.-E. Fu, in *2011 11th IEEE International Conference on Nanotechnology (IEEE-NANO 2011)*, p. 541.
14. D. Barreca, A. Milanov, R.A. Fischer, A. Devi, and E. Tondello, *Surf. Sci. Spectra* 14, 34 (2007).
15. S. Suzer, S. Sayan, M.M. Banaszak Holl, E. Garfunkel, Z. Hussain, and N.M. Hamdan, *J. Vac. Sci. Technol.* 21, 106 (2003).
16. M. Lanza, G. Bersuker, M. Porti, E. Miranda, M. Nafría, and X. Aymerich, *Appl. Phys. Lett.* 101, 193502 (2012).
17. A. Katsman, G. Zeevi, and Y. Yaish, *MRS Adv.* 1, 349 (2016).
18. C. Mannequin, P. Gonon, C. Vall, L. Latu-Romain, A. Bsiesy, H. Grampeix, A. Salaun, and V. Jousseaume, *J. Appl. Phys.* 112, 074103 (2012).
19. G. Bersuker, D.C. Gilmer, D. Veksler, P. Kirsch, L. Vandelli, A. Padovani, L. Larcher, K. McKenna, A. Shluger, V. Iglesias, M. Porti, and M. Nafría, *J. Appl. Phys.* 110, 124518 (2011).
20. S. Clima, Y.Y. Chen, R. Degraeve, M. Mees, K. Sankaran, B. Govoreanu, M. Jurczak, S. De Gendt, and G. Pourtois, *Appl. Phys. Lett.* 100, 33102 (2012).
21. J. McPherson, J.Y. Kim, A. Shanware, and H. Mogul, *Appl. Phys. Lett.* 82, 2121 (2003).